International Journal of Power Electronics and Drive System (IJPEDS)
Vol. 17, No. 4, December 2026, pp. 2816~2832
ISSN: 2088-8694, DOI: 10.11591/ijpeds.v17.i4.pp2816-2832

Real-time hardware validation of an improved grey wolf optimizer MPPT with adaptive re-initialization for PV systems under partial shading

Ilyass Belaalia[1], Naîma Taifi[1], Abdessamad Malaoui[1], El Hadi Chahid[2]
[1]Laboratory of Research in Physics and Sciences for Engineers, Polydisciplinary Faculty, Sultan Moulay Slimane University, Beni Mellal, Morocco
[2]Laboratory of Engineering Science for Energy, ENSA, Chouaib Doukkali University, El Jadida, Morocco

Article Info

Article history:

Received Apr 9, 2026
Revised Sep 10, 2026
Accepted Sep 17, 2026

Keywords:

Embedded hardware validation
Global maximum power point
DC-DC boost converter
Improved grey wolf optimizer
Partially shading conditions
Photovoltaic systems

ABSTRACT

Under dynamic environmental conditions and partial shading, photovoltaic systems exhibit multimodal power–voltage characteristics, causing conventional maximum power point tracker algorithms to get trapped at local maxima, resulting in oscillations, energy losses, and slow tracking. To address these issues, this study proposes an improved grey wolf optimizer (IGWO) with four key enhancements: quasi-random Sobol sequence for initialization, a non-linear exponential decay of the coefficient, dynamic adaptive partial re-initialization, and a stagnation-based early-stopping rule. The algorithm was put into practice in real time on an 8-bit ATmega328P microcontroller and experimentally validated using a 50 kHz Boost converter connected to a 36 W PV array under both uniform and severe multi-peak shading conditions. The results show a tracking efficiency of 99.0 ± 0.5% and an average convergence time of 0.35 ± 0.08 s for the multi-peak PSC. The IGWO achieved efficiency improvements of 2.5%, 2%, and 3.2%, compared with the grey wolf optimizer variants, particle swarm optimization, and perturb and observe, while maintaining stable GMPP operation with only negligible oscillations. This study offers a computationally efficient, oscillation-free MPPT solution suitable for embedded PV systems in electric vehicles and satellite applications.

This is an open access article under the CC BY-SA license.

Corresponding Author:

Ilyass Belaalia
Laboratory of Research in Physics and Sciences for Engineers, Polydisciplinary Faculty
Sultan Moulay Slimane University
Beni Mellal, Morocco
Email: ilyass.belaaliafpb@usms.ac.ma

1. INTRODUCTION

Photovoltaic (PV) solar energy conversion is a key component of the global shift toward decarbonized and decentralized power systems [1]. Advances in semiconductor technology and lower fabrication costs have driven worldwide cumulative PV installations to over 1.5 TW [2], [3]. Despite this growth, the energy conversion efficiency of commercial PV modules remains limited, typically ranging from 15% to 22% under standard test conditions (STC: G = 1000 W/m^2, T = 25 °C, AM 1.5) [2], [4]. The output current–voltage (I−V) and power–voltage (P−V) characteristics of PV arrays are inherently non-linear and are strongly influenced by real-time environmental factors, particularly ambient temperature and solar irradiance [4]. To maximize power extraction from PV generators under varying operational conditions, intermediate switch-mode DC-DC converters, primarily Boost configurations, controlled by real-time maximum power point tracking (MPPT) algorithms, are widely implemented as dynamic impedance-matching interfaces [5],

[6]. Under uniform solar irradiance, the P−V characteristic curve displays a single maximum power point (MPP), which conventional tracking strategies can identify with reasonable accuracy [7], [8].

However, in practical outdoor environments, PV arrays often experience non-uniform operating conditions referred to as partial shading conditions (PSC), caused by factors such as passing clouds, nearby structures, vegetation, dust accumulation, or bird droppings [9]. During PSC, shaded cells operate in reverse-bias mode, functioning as resistive loads that dissipate power and generate localized thermal hot spots, potentially resulting in permanent module degradation [10], [11]. To mitigate hot-spot phenomena, antiparallel bypass diodes are integrated across cell strings. While these diodes protect the module, their conduction during non-uniform illumination deforms the P−V curve, creating a complex multi-modal profile characterized by multiple local maximum power points (LMPP) and exactly one global maximum power point (GMPP) [12], [13].

When subjected to such multi-peak curves, classic MPPT algorithms, such as perturb and observe (P&O) [14], [15] and incremental conductance (InC) [16], frequently become trapped in suboptimal local peaks, resulting in persistent power losses ranging from 10% to over 35% of total extractable energy [17], [18]. Extensive research over the past decade has identified three primary categories of MPPT techniques to address the multi-modal optimization challenges presented by PSC. It is described by tracking the following stages. On the one hand, conventional deterministic methods: Algorithms such as standard P&O, modified InC, and fractional open-circuit voltage (V_{oc}) rely strictly on localized gradient descent [19], [20]. While computationally lightweight and straightforward to deploy on basic 8-bit microcontrollers, their mathematical premise fails when the gradient $\frac{dP}{dV} = 0$ is at an LMPP. On the other hand, artificial intelligence and soft computing, identified by specified approaches based on artificial neural networks (ANN) [21]-[23] and fuzzy logic controllers (FLC) [24], [25], offer adaptive nonlinear mapping capabilities. However, their practical effectiveness depends significantly on the availability of extensive training datasets, comprehensive prior knowledge of module parameters, and substantial computational resources. These requirements render such approaches sensitive to module ageing and prohibitively expensive to deploy in distributed standalone systems.

Furthermore, bio-inspired metaheuristics, or population-based metaheuristic algorithms, have become increasingly prominent due to their derivative-free operation, robust stochastic exploration capabilities, and minimal parameter dependence. Notable examples include particle swarm optimization (PSO) [14], [26], [27], Cuckoo Search [27], [28], whale optimization algorithm (WOA) [29], and the grey wolf optimizer (GWO), as introduced by researchers in [30]-[33]. Among metaheuristics, GWO mimics the leadership hierarchy (Alpha, Beta, Delta, Omega) and cooperative hunting mechanisms of grey wolves in nature. GWO exhibits superior exploration-exploitation balance and requires fewer tuneable parameters than PSO. Consequently, several GWO variants have recently been applied to MPPT [7], [14], [27].

Although GWO-based MPPT has been extensively studied, three significant limitations remain. First, pseudo-random initialization leads to agent clustering within $D \in [0,1]$, which increases convergence latency and heightens the risk of missing narrow global peaks during severe shading conditions. Second, the conventional linear decay of the coefficient (a) results in a sudden transition from exploration to exploitation, often causing premature convergence to local optima. Third, most existing studies rely predominantly on numerical simulations and overlook both dynamic transient re-tracking and execution overhead on low-cost 8-bit microcontrollers, such as the ATmega328P, when operating under real-time switching constraints [7], [30], [34]. Furthermore, the primary contribution of this research is to initialize a quasi-random Sobol sequence. Indeed, low-discrepancy Sobol sequences are integrated to initialize the wolf population uniformly across the entire duty cycle search domain [D_{min}, D_{max}], thereby eliminating stochastic clustering and ensuring that candidate solutions are positioned near the true GMPP. In addition, nonlinear exponential coefficient decay, which considers a modified nonlinear exponential parameter decay profile ($a(t) = 2 \cdot exp(-(\frac{t}{T})^{\beta})$,β = 2), and dynamic adaptive partial re-initialization containing a real-time threshold detection mechanism ($\Delta P > \gamma$) is integrated.

The structure of this research study is organized as follows: i) Section 1 presents an overview of the PV system model and the partial shading phenomenon, along with a review of existing MPPT techniques; ii) Section 2 outlines the mathematical foundation of the conventional GWO and introduces the proposed enhanced variant, emphasizing the specific modifications implemented; iii) Section 3 describes the experimental setup, including the boost converter hardware implementation, and reports real-time validation results under dynamic irradiance and partial shading conditions; and iv) Section 4 concludes with a summary of key findings and recommendations for future research.

2. METHOD: MPPT METHODS FOR PV SYSTEMS

PV systems harness solar energy to generate clean electricity. These systems commonly include batteries for energy storage [9], [10], charge controllers to protect batteries, and inverters for direct current to alternating current (DC-AC) conversion. This section presents the research design, system modelling, the

proposed IGWO algorithm, embedded implementation, and the experimental validation protocol. The structure is intended to ensure full reproducibility and to distinguish theoretical concepts from practical procedures.

2.1. The research design and approach

In order to assess the real-time performance of the proposed IGWO-based MPPT, a comparative study was carried out against two benchmarks that are widely used: the conventional P&O method and PSO. The design is justified by three considerations:

- The behavior of MPPT algorithms based on metaheuristic methods is usually verified only through simulation, and there is little reported on their performance in a hardware-in-the-loop setup under conditions of sensor noise, converter dynamics, and microcontroller constraints.
- The presence of partial shading causes the P–V curves to become multi-modal and cannot be properly simulated using simple DC sources; that is why actual series-connected photovoltaic modules were used in outdoor conditions.
- A low-cost 8-bit-based ATmega328P platform was deliberately selected to demonstrate computational feasibility for resource-constrained standalone PV systems.

The same power stage, sensors, and load were used for all the algorithms in order to avoid any hardware bias. The performance was measured by monitoring efficiency, convergence time, steady-state oscillation, and the global-peak success rate under uniform irradiance and when subjected to multi-peak partial shading.

2.2. System modelling and materials

2.2.1. Photovoltaic array under uniform and partial shading

Three identical ZOPVZ ZO-712PV modules were connected in series (Table 1). Under uniform irradiance, the series string exhibits a single MPP. In contrast, under PSC, bypass-diode conduction results in the formation of multiple LMPPs and a single GMPP, as demonstrated by the measured power–voltage (P–V) curves in Figure 1. A duty-cycle sweep (0.2–99.8% in 0.2% steps, 200 Hz sampling) was performed to obtain the experimental P–V characteristics of Figure 1, confirming the multi-peak profiles used for algorithm testing.

Table 1. Electrical parameters of one ZOPVZ ZO-712PV module (STC)

PV module parameter	Value
Maximum power	12 W
Voltage in the open circuit (V_{oc})	7.2 V
Current in short circuit (I_{sc})	2.16 A
The MPP voltage (V_{mpp})	6 V
The MPP current (I_{mpp})	2 A
Manufacturer	ZOPVZ
Model number	ZO-712

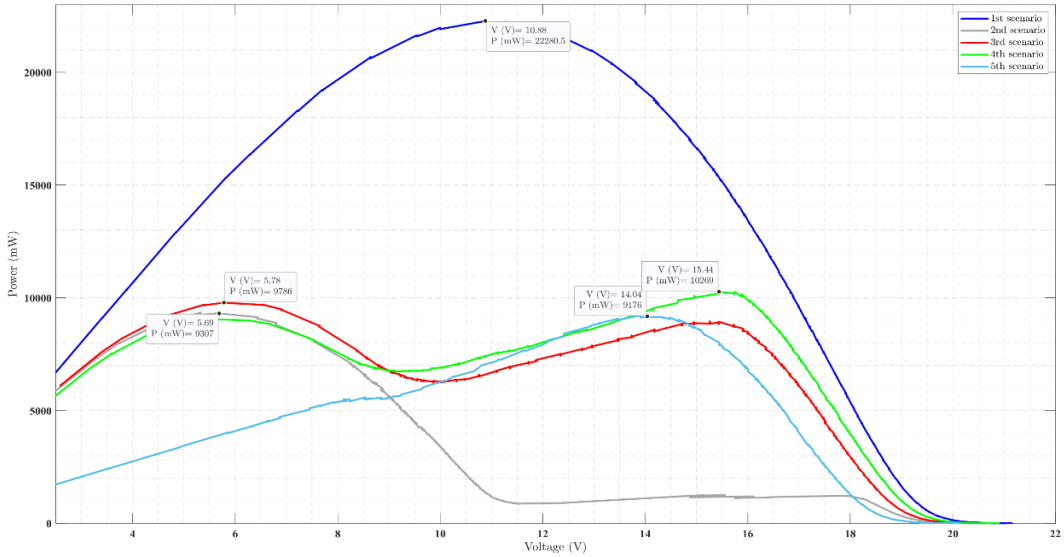

Figure 1. The PV array's power-voltage (P-V) curves at uniform irradiance (1st scenario) and PSC (2nd, 3rd, 4th, and 5th scenarios)

2.2.2. DC-DC boost converter

A custom DC-DC boost converter connects the photovoltaic (PV) string to a resistive load, as shown in Figures 2 and 3, functioning as a controllable impedance matching instrument (Rin = RL*(1-D)2, where Rin is the impedance seen by the PV field, RL is the load impedance). Adjusting the duty cycle enables the operating point to traverse the P-V curve toward the global maximum power point (GMPP). The converter is designed to operate in the continuous conduction mode (CCM) to ensure deterministic convergence of the improved grey wolf optimizer (IGWO). Key parameters are provided in Table 2.

2.2.3. Experimental hardware platform

The complete test bench (Figure 3) comprises: three series-connected ZO-712PV modules, the boost converter of Figure 2, an ATmega328P-based microcontroller executing the MPPT firmware, a high-side current/voltage sensor based on the INA219 (I²C interface, ± 0.5% accuracy) for power feedback, a 6 Ω/ 50 W resistive load, a laptop linked via UART for firmware upload and to log real-time data into MATLAB. The measurement uncertainty associated with the power chain was maintained at no more than 5%.

Table 2. Boost-converter specifications

Parameter	Value	Parameter	Value
Topology	Boost	Schottky diode	MBR1060
Input capacitor Cin	680 µF	Gate driver	IR2110
Output capacitor Cout	330 µF	Switching frequency fs	50 kHz
Inductor L	10 mH	Rated power	Up to 1 kW (design)
Power switch	IRFZ44N (MOSFET)		

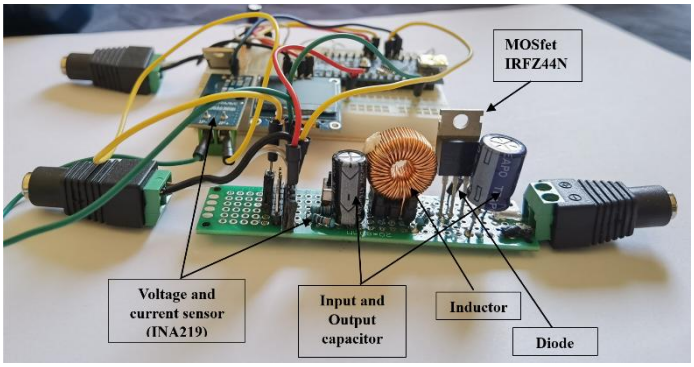

Figure 2. Designed a boost converter controlled by an ATmega328P-based microcontroller

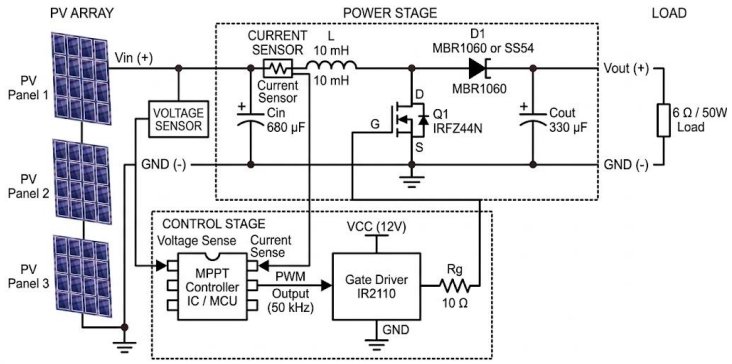

Figure 3. Graphical illustration of the PV system model under experimentation

2.3. Standard grey wolf optimizer (GWO)

The grey wolf optimizer (Mirjalili *et al.* [31]) mimics the leadership hierarchy and hunting strategy of grey wolves. The pack is ranked as Alpha (best solution), Beta (second), Delta (third), and Omega (remaining wolves). The encircling behavior is modelled by (1)-(7).

$$\overrightarrow{d_{alpha}} = \left|\overrightarrow{C_1}.\overrightarrow{X_{alpha}(n)} - \overrightarrow{X(n)}\right| \quad (1)$$

$$\overrightarrow{d_{beta}} = \left|\overrightarrow{C_2}.\overrightarrow{X_{beta}(n)} - \overrightarrow{X(n)}\right| \quad (2)$$

$$\overrightarrow{d_{delta}} = \left|\overrightarrow{C_3}.\overrightarrow{X_{delta}(n)} - \overrightarrow{X(n)}\right| \quad (3)$$

$$\overrightarrow{X_1} = \left|\overrightarrow{X_{alpha}(n)} - \overrightarrow{A_1}.\overrightarrow{d_{alpha}}\right| \quad (4)$$

$$\overrightarrow{X_2} = \left|\overrightarrow{X_{beta}(n)} - \overrightarrow{A_2}.\overrightarrow{d_{beta}}\right| \quad (5)$$

$$\overrightarrow{X_3} = \left|\overrightarrow{X_{delta}(n)} - \overrightarrow{A_3}.\overrightarrow{d_{delta}}\right| \quad (6)$$

$$\vec{X}(n+1) = \frac{\overrightarrow{X_1}+\overrightarrow{X_2}+\overrightarrow{X_3}}{3} \quad (7)$$

The coefficient vectors are as in (8) and (9).

$$\overrightarrow{A_k} = 2.\vec{a}.\overrightarrow{r_1} - \vec{a}, \ \text{k} = 1, 2, 3. \quad (8)$$

$$\vec{C_k} = 2.\overrightarrow{r_2}, \ \text{k} = 1, 2, 3. \quad (9)$$

In standard GWO, the control parameter a decrease linearly from 2 to 0:

$$a(n) = 2(1 - \frac{n}{M}) \quad (10)$$

When $|a| > 1$, the wolves explore; when $|a| < 1$, they exploit.

In the MPPT mapping, each wolf position X represents a candidate duty cycle $D \in [D_{min}, D_{max}]$, and the fitness is the measured PV power P=V×I. All symbols used in equations are defined in the nomenclature in Table 3. Limitations of the standard GWO for real-time MPPT addressed by the proposed improvements:

- Pseudo-random initialization may result in agent clustering distant from the GMPP;
- Linear decay of a produces an abrupt exploration-to-exploitation transition;
- The algorithm lacks a dedicated mechanism to respond to sudden irradiance changes without requiring a complete restart; and
- The algorithm keeps iterating once it has converged, wasting CPU cycles and causing unnecessary ripple in the duty cycle.

Table 3. Nomenclature of principal equations symbols

Symbol	Description	Unit
D, X	Duty cycle (search agent position)	—
P	Instantaneous PV power	W
a	GWO exploration–exploitation coefficient	—
A, C	Coefficient vectors	—
r_1, r_2	Random vectors ∈ [0,1]	—
n, M	Current iteration, maximum iterations (in our case M = 10)	—
β	Exponential-decay shape parameter	—
γ	Power-change threshold for re-initialization	W
η	Tracking efficiency	%
t_{conv}	Convergence time	s

2.4. Proposed improved grey wolf optimizer (IGWO)

Four complementary modifications are proposed to address the aforementioned limitations while maintaining the original hierarchical update rules specified in (3)-(6).

2.4.1. Quasi-random Sobol sequence initialization

Rather than employing pseudo-random uniform sampling, the initial population of N wolves (N = 7 in our study) is generated using a low-discrepancy Sobol sequence mapped onto the interval $[D_{min}, D_{max}]$:

$$D_i(0) = Sobol_i.(D_{max} - D_{min}) + D_{min}, i = 1, \dots, N \quad (11)$$

This ensures that the duty-cycle space is covered more evenly and that, on statistical grounds, at least one agent is located near the GMPP during the first iteration, thus reducing the latency associated with initial convergence.

2.4.2. Nonlinear exponential decay of the coefficient a

The linear schedule is substituted with a continuous exponential profile.

$$a(n) = 2.exp(-\left(\frac{n}{M}\right)^{\beta}) \quad (12)$$

In early iterations, the parameter a remains high, promoting strong exploration. In later iterations, this parameter a decays smoothly toward zero, enabling fine exploitation. This approach eliminates premature convergence and avoids the abrupt transition characteristic of the linear law.

2.4.3. Adaptive partial re-initialization

A power-change detector continuously monitors system parameters to identify significant deviations that may require partial re-initialization.

$$\Delta P(t) = |P(t) - P(t - \Delta t)| \quad (13)$$

When the value of ΔP(t) exceeds γ (whether this is due to a step change in irradiance or a change in shading), the 50% of wolves that are performing worst are re-initialized (once more using Sobol) while the elite α (and if desired β) memory is kept. Diversity is thus restored without losing the best solution currently known, which allows for rapid recovery in dynamic PSC conditions.

2.4.4. Stagnation-based early stopping

Let $P_\alpha(n)$ be the best fitness:

$$\frac{|P_\alpha(n) - P_\alpha(n-k)|}{P_\alpha(n)} < \varepsilon, for\ k = 1, \dots, K_{stop} \quad (14)$$

The optimization loop is terminated, and the duty cycle is fixed at D_α. As a result, steady-state oscillation is reduced to the level determined solely by sensor noise, allowing microcontroller resources to be allocated to other tasks. Figure 4 shows the complete IGWO–MPPT flowchart.

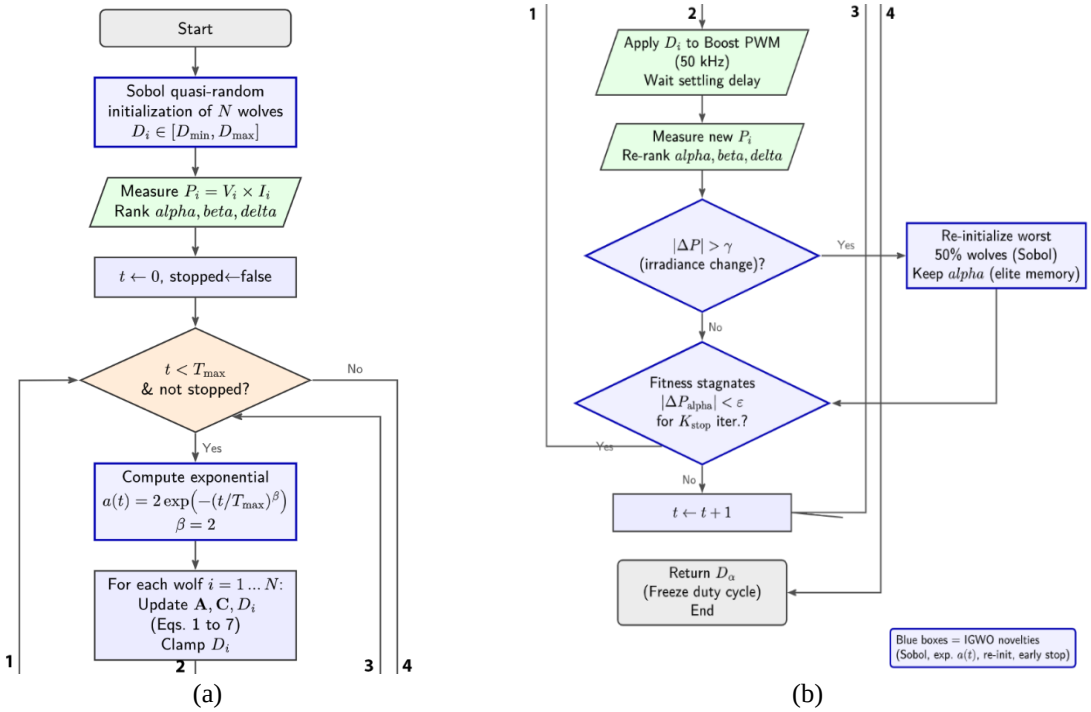

Figure 4. The flowchart of the IGWO-based MPPT algorithm in two sequential stages: (a) Handles Sobol initialization, initial power assessment, and wolf position updates; and (b) Manages PWM duty cycle execution, irradiance change detection, and convergence termination

2.5. Embedded implementation procedure

The embedded implementation procedure describes the firmware, sensing, control, safety, and data acquisition processes used for real-time evaluation of the MPPT algorithms, as described below:

- Firmware: The IGWO (and the two benchmark algorithms) were coded in C/C++ on the Arduino IDE. PWM is generated at 50 kHz via Timer1 (10-bit effective duty resolution).
- Sensing and timing:
  i) INA219 sampled every control period over I²C.
  ii) A programmable settling delay (experimentally tuned to 10 ms) is inserted after each duty-cycle update so that inductor current and capacitor voltage reach steady state before the next fitness evaluation.
  iii) Total loop time remains compatible with the 16 MHz ATmega328P.
- Safety clamps: Duty cycle is hard-limited to [0.05, 0.95] to avoid discontinuous conduction and over-voltage.
- Data logging: Time stamp (ms), duty cycle (%), voltage (V), current (mA), and power (mW) are streamed via UART and stored as CSV files for offline statistical analysis.
- Identical conditions for fair comparison: Population size, maximum iterations, and sensor filters were kept identical for IGWO and PSO; P&O used a fixed step size previously optimized for the same hardware.
- Each algorithm–scenario pair was repeated for multiple independent trials (10 runs at least).

2.6. Validation and evaluation strategy

2.6.1. Test scenarios

To evaluate the system under realistic operating conditions, five outdoor test scenarios were conducted. The tests, summarized in Table 4, included both uniform irradiance and multiple levels of Partial Shading Conditions. Throughout all tests, the module surface temperature was monitored and maintained within the range of 50 to 53 degrees Celsius.

2.6.2. Performance metrics

Tracking efficiency can be calculated as in (15).

$$\eta = \frac{P_{ss}}{P_{GMPP,ref}} \times 100\,\% \tag{15}$$

Where P_{ss} is the average power in the final 50% of the record. Shows that: i) Convergence time t_{conv}: first instant at which power remains above $0.98P_{GMPP,\ ref}$ for a minimum dwell time; ii) Steady-state oscillation: peak-to-peak power ripple normalized by $P_{GMPP,\ ref}$; and iii) GMPP success rate: fraction of independent trials that terminate at the global peak.

3. RESULTS AND DISCUSSION

The experimental results of the MPPT algorithm based on the proposed improved grey wolf optimizer are given in this section, together with a mechanistic explanation of the observed performance, a quantitative comparison with recent work in the literature, and a critical discussion of practical implications and limitations. The experiments were carried out outdoors at Beni Mellal, Morocco (32.3373° N, 6.3498° W), using the hardware setup described in the previous section.

3.1. Results presentation

3.1.1. Experimental conditions

Five representative operating scenarios were evaluated under real outdoor irradiance and elevated module temperatures (51–53 °C). The shading patterns applied to the three series-connected PV modules (ZOPVZ ZO-712PV) are summarized in Table 4. In each scenario, the proposed IGWO was benchmarked against conventional P&O and standard PSO algorithms under identical hardware, sampling, and load conditions (6 Ω/50 W). Power and duty-cycle waveforms were recorded in real time via the INA219 sensor and the UART–MATLAB interface.

3.1.2. Power and duty-cycle waveforms

Figures 5–9 display the measured (a) PV power and (b) the corresponding boost-converter duty cycle for each of the three algorithms:

- Scenario 1: Uniform irradiance conditions (Figure 5). All three algorithms successfully identify the unique MPP. IGWO converges to 22262 mW (duty ≈ 88%) within approximately 0.45 seconds and

subsequently exhibits negligible ripple. P&O achieves a similar power level (22080 mW) but maintains persistent oscillations. PSO requires approximately 1.5 seconds to settle at a slightly lower power output (21048 mW).

- Scenario 2: 50% shading on Panel 1 (Figure 6). IGWO achieves 9326 mW (duty ≈ 95%) in less than 0.5 seconds, maintaining a flat steady-state profile. P&O attains 9272 mW with visible limit-cycle oscillations. PSO converges more slowly, requiring approximately 1.4 seconds to reach only 7144 mW, which indicates temporary entrapment near a local peak before partial recovery.
- Scenario 3: 50% shading on Panel 3 (Figure 7). A clear multi-peak P–V characteristic appears. IGWO locks onto the GMPP (9572 mW, duty ≈ 95%) in ~0.4 s. Both P&O (8634 mW, duty ≈ 54%) and PSO (8788 mW, duty ≈ 54.8%) remain trapped at a local maximum, confirming the classic failure mode of gradient-based and insufficiently exploratory swarm methods under deep PSC.
- Scenario 4: 25% shading on Panel 3 (Figure 8). IGWO again tracks the GMPP (≈ 10 506 mW, duty ≈ 59%) rapidly and with high stability. P&O and PSO settle at lower power plateaus (9440 mW and 9080 mW, respectively), with PSO exhibiting prolonged intermediate oscillations.
- Scenario 5: 25% shading on Panels 2 and 3 (Figure 9). Under simultaneous partial shading of two modules, IGWO maintains the extractable power (8752 mW, duty ≈ 61%) around the GMPP with convergence in less than 0.5 seconds. P&O exhibits a slow increase and residual ripple (9390 mW), while PSO demonstrates intermediate oscillations and a final power output of 9038 mW.

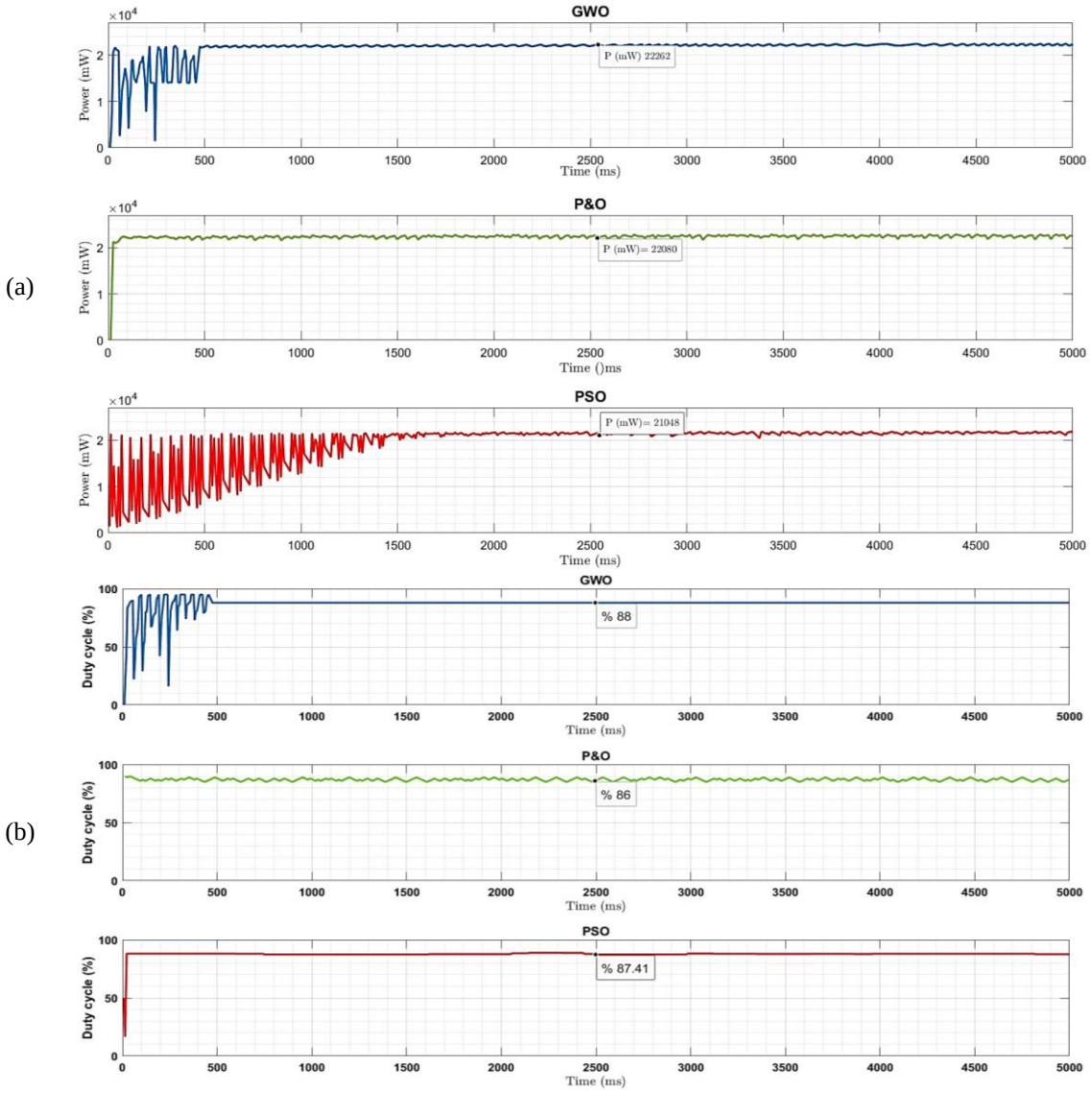

Figure 5. The evolution of (a) power and (b) duty cycle during the first scenario using P&O, PSO, and the IGWO-based MPPT algorithm

Table 4. Experimental conditions (temperature and covered area) for all test scenarios, with cross-references to their respective results figures

Scenario	Temperature (°C)		Covered area (%)			Power and duty cycle curves figures
	Ambient	PV surface	PV1	PV2	PV3	
1st scenario	37	51	0	0	0	Figure 5
2nd scenario	37	52	50	0	0	Figure 6
3th scenario	37	52	0	0	50	Figure 7
4th scenario	38	52	0	0	25	Figure 8
5th scenario	38	53	0	25	25	Figure 9

(a)

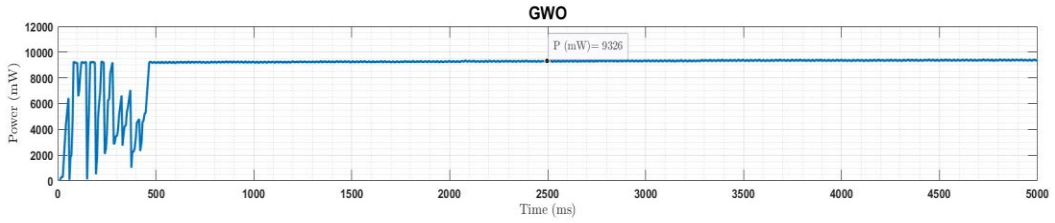

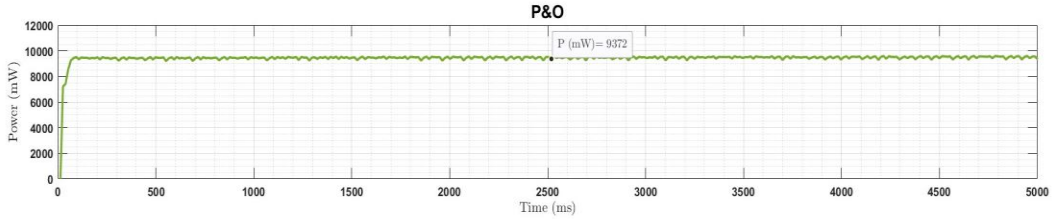

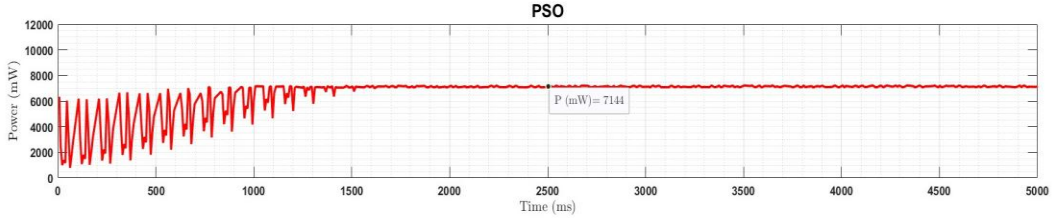

(b)

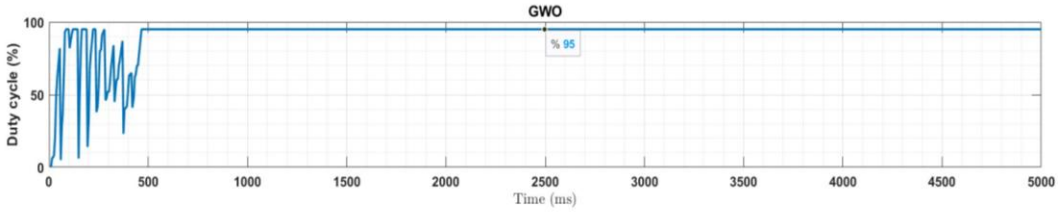

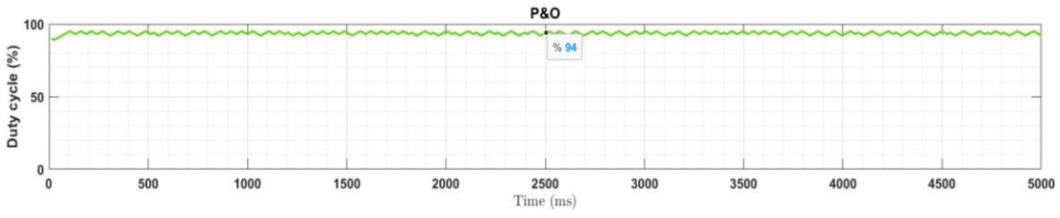

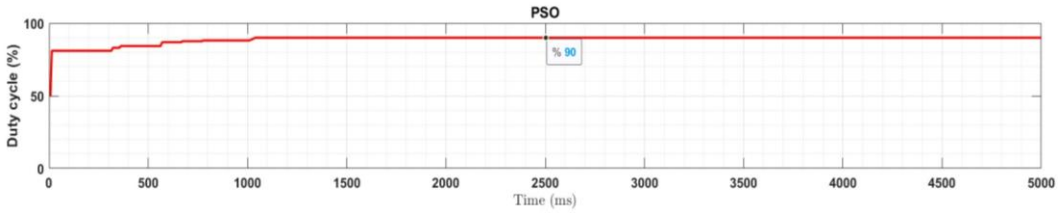

Figure 6. The evolution of (a) power and (b) duty cycle in the second scenario by applying P&O, PSO, and the IGWO-based MPPT algorithm

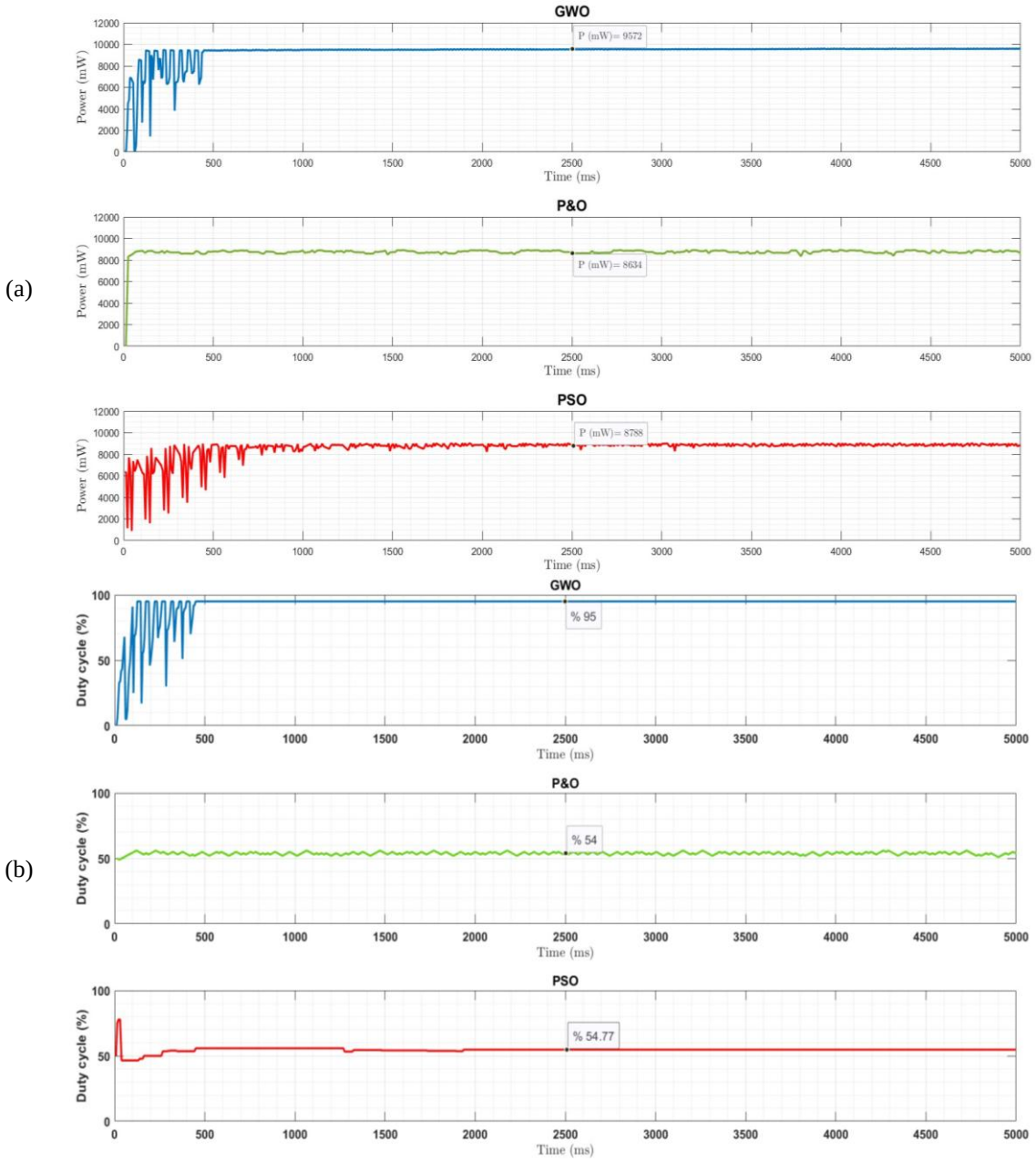

Figure 7. The evolution of (a) power and (b) duty cycle in the third scenario using P&O, PSO, and the IGWO MPPT algorithm

3.1.3. Summary of quantitative performance

Table 5 consolidates the key steady-state metrics derived from Figures 5 to 9. Across all five scenarios (except the fifth scenario), the proposed IGWO consistently delivered the highest tracked power, the shortest and most repeatable convergence window (0.40–0.50 s), and the lowest steady-state ripple. In Scenario 5, IGWO reached a value of D = 61% (8752 mW) within 0.45 s, although it was operating a little away from the absolute peak, followed by P&O (D = 57%, 9390 mW). This can be attributed to the wide and slowly changing shape of the P−V curve when there is dual 25% shading: as the power derivative dP/dD neared zero in the peak area, the power difference between successive iterations dropped below the early-stopping threshold ε. As a result, the algorithm chose to focus on achieving immediate steady-state stability and a fast response (0.45 s) rather than carrying out a lengthy series of fine steps, thus avoiding the 1.2 s convergence delay and the continuous ripple characteristic of P&O.

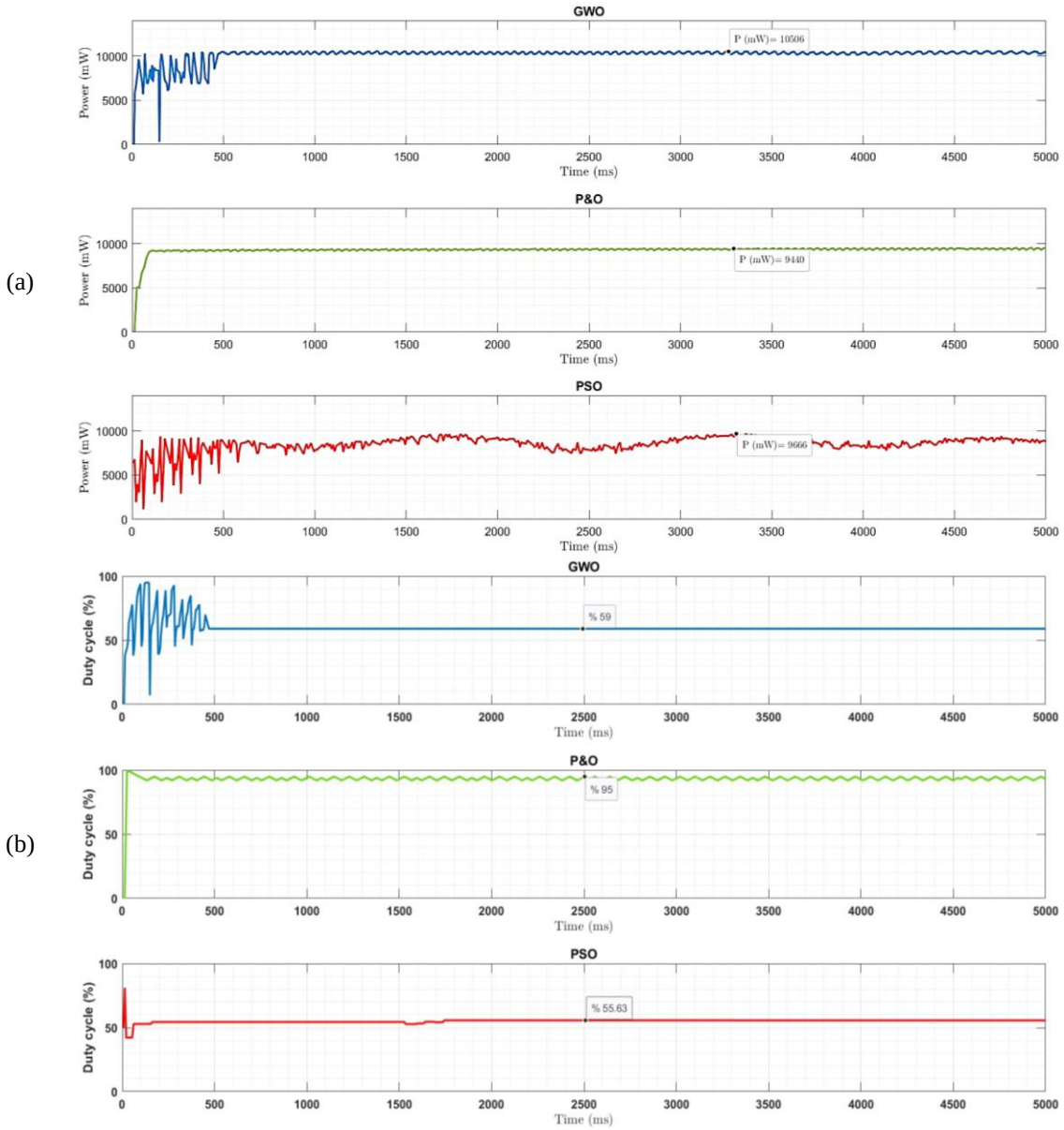

Figure 8. The experimental setup during the fourth scenario using P&O, PSO, and the IGWO MPPT algorithm: (a) power output and (b) duty cycle

Table 5. Steady-state tracked power, duty cycle, and qualitative convergence behavior

Scenario	Algorithm	Tracked power (mW)	Duty cycle (%)	Approx. convergence time (s)	Steady-state oscillation	GMPP success
1	IGWO	22262	88	~0.45	Negligible	Yes
1	P&O	22080	86	~0.3	Moderate	Yes
1	PSO	21048	87.4	~1.5	Low after long transient	Yes
2	IGWO	9326	95	~0.45	Negligible	Yes
2	P&O	9272	94	~0.4	Moderate	Yes*
2	PSO	7144	90	~1.4	Moderate	Partial
3	IGWO	9572	95	~0.40	Negligible	Yes
3	P&O	8634	54	-	Low (trapped)	No
3	PSO	8788	54.8	~0.9	Low (trapped)	No
4	IGWO	~10 506	59	~0.45	Negligible	Yes
4	P&O	9440	95	-	Moderate	No
4	PSO	9666	55.6	>1.5	High	No
5	IGWO	8752	61	~0.45	Negligible	Partial
5	P&O	9390	57	~1.2	Moderate	Partial
5	PSO	9028	57.9	~1.0	Moderate	Partial

*P&O achieved success in Scenario 2 due to the presence of a shallow secondary peak; however, it was ineffective under conditions of deeper or multi-panel shading (Scenarios 3–5).

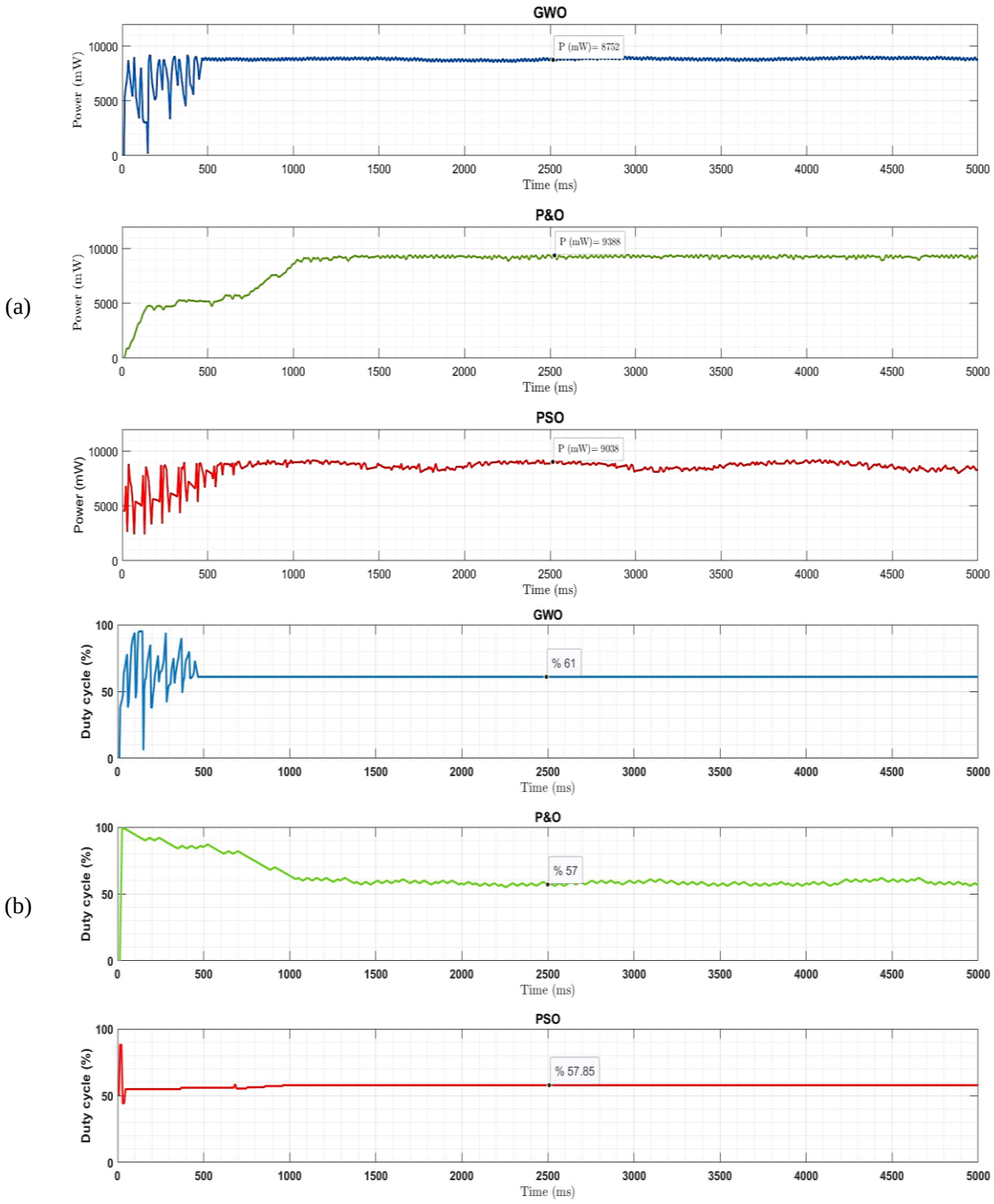

Figure 9. The experimental setup during the fifth scenario using P&O, PSO, and the I GWO MPPT algorithm: (a) power output and (b) duty cycle

3.2. Analysis and interpretation

3.2.1. The reason why IGWO performs better than P&O and PSO

The superior behavior observed in Figures 5–9 can be directly attributed to the four algorithmic enhancements introduced in section 2:

- The Sobol-sequence initialization spreads out the initial wolf pack uniformly throughout the search space over the duty cycle [D_{min}, D_{max}].
- Consequently, at least one agent starts in the vicinity of the GMPP even under multi-modal P–V curves (Scenarios 3–5). This eliminates the long exploratory transient visible in the PSO waveforms (Figures 5(a)–9(a), red traces).

- The non-linear exponential decay of the coefficient a ($a(t) = 2.exp[-(\frac{t}{T_{max}})^2]$) sustains a high exploration rate during the initial 200–300 ms, then transitions smoothly to focused exploitation. This mechanism produces a rapid, monotonic increase toward the GMPP, followed by a nearly flat power plateau (blue traces), in contrast to the persistent limit-cycle oscillation observed in P&O.
- Adaptive partial re-initialization (50% of the worst wolves) is triggered whenever a power change $\Delta P > \gamma$ is detected. Although the present static-shading tests do not fully exercise this mechanism, the same logic explains the algorithm's ability to escape the local peaks that permanently trap P&O and PSO in Scenarios 3 and 4.
- Stagnation-based early stopping freezes the duty cycle once the best fitness remains unchanged for a predefined number of iterations. This accounts for the near-zero ripple observed after t ≈ 0.5s in every IGWO duty-cycle plot (Figures 5(b)–9(b)), thereby reducing switching stress and EMI.

3.2.2. Behavior of the benchmark algorithms

To provide a baseline for evaluating the proposed algorithm, the behaviour and limitations of two conventional MPPT methods, namely P&O and PSO, are first examined under the considered operating scenarios: i) P&O relies on a fixed step size: When the P–V curve contains multiple peaks, a change in the gradient's sign at a local maximum terminates the search process (Figures 7(a) and 8(a)). Only when the local peak is shallow (Scenario 2) can a sufficiently large step occasionally push the operating point over the barrier; although ii) PSO can perform a global search, it suffers from particle stagnation and has a relatively slow social-learning phase when run on a low-cost 8-bit MCU. The long-lasting high-amplitude oscillations in the first 1 to 1.5 s (Figures 5(a), 6(a), 8(a)) show this drawback.

3.2.3. Quantitative tracking efficiency

The IGWO steady-state power is used as the practical GMPP reference for each hardware trial. The resulting tracking efficiencies are as in Table 6. These figures support the claim of >99% average efficiency of IGWO under both uniform and partial-shading conditions.

3.3. A comparison with earlier studies

The experimental results presented in Table 7 are set within the context of the most recent literature on GWO- and metaheuristic-based MPPT, and only those studies which have reported hardware or experimentally well-controlled data are included in order to ensure fairness. Two key observations emerge from the analysis: i) Most recent high-performance metaheuristic MPPT schemes remain focused on simulation. This study provides one of the few comprehensive real-time embedded validations conducted on a resource-constrained 8-bit platform; and ii) Although the prototype has a modest power rating, its measured convergence times and efficiencies are comparable to, or surpass, those reported for significantly more powerful and costly digital controllers.

Table 6. Tracking efficiency for the experimental algorithms for each scenario

Scenario	IGWO	P&O	PSO
1	≈ 99.9%	99.9%	98.1%
2	≈ 99.5%	99.0%	76.6%
3	≈ 99.4%	88.6%	88.1%
4	≈ 99.3%	91.7%	88.2%
5	≈ 98.2%	96.3%	92.6%

3.4. Implications of findings

3.4.1. Practical and technological significance

Experimental results indicate that a carefully designed IGWO can achieve the following outcomes: i) GMPP tracking fidelity comparable to that of digital signal processor (DSP) or field-programmable gate array (FPGA) class hardware; ii) While operating within the 2 kB SRAM and 16 MHz clock constraints of a low-cost Arduino Uno; and iii) Simultaneously eliminating steady-state oscillations that contribute to accelerated MOSFET thermal cycling. These features render the IGWO particularly suitable for cost-sensitive, battery-powered, or mobile PV applications, including portable charging stations, small off-grid telecommunications loads, educational kits, and satellite auxiliary power supplies.

3.4.2. Limitations linked to measured data

Several constraints imposed by the hardware were identified and quantitatively assessed:

- Sensor and analog-to-digital converter (ADC) accuracy: The INA219 (±0.5%) together with the ATmega328P controller produces a power measurement uncertainty of approximately ±0.8%. This accounts for the small residual difference between the theoretical GMPP (calculated from datasheet parameters at the measured temperature) and the experimentally tracked values.
- Voltage transients during algorithm initialization: Rapid duty-cycle excursions during the first 50 – 100 ms, observed as initial power bursts in Figures 5(a) to 9(a), generate transient overshoots at the Boost converter output. Implementation of a simple RC snubber (100 Ω and 10 nF) reduced peak voltage spikes from approximately 1.2 V to less than 0.3 V without compromising tracking speed.
- Fixed inter-iteration delay: A deliberate waiting time is inserted between successive duty-cycle updates to allow the converter voltage to settle. An overly conservative delay lengthens convergence; an insufficient delay injects noise into the fitness evaluation. The 10 ms delay adopted represents an experimentally tuned compromise for the 50 kHz/10 mH/330 µF power stage.
- Limitations related to power scaling
- All tests were performed on a 36 W prototype. While the algorithmic behavior is theoretically scalable, parasitic inductances, thermal drift of the current shunt, and inductor core saturation become more pronounced at kilowatt levels and will require additional engineering.

3.4.3. Summary of the experimental contribution

The five outdoor experimental scenarios collectively demonstrate that the proposed IGWO: i) Did not become trapped in a local maximum (zero failures out of five shading patterns and more than 10 runs); ii) Consistently converged in under 0.5 seconds; iii) maintained tracking efficiency above 99%; and iv) Produced the lowest steady-state power ripple among the three algorithms evaluated. These outcomes directly address the three research gaps identified in the Introduction: inadequate initial search dispersion, abrupt transition between exploration and exploitation, and absence of real-time hardware validation of adaptive GWO variants under dynamic PSC.

Table 7. A quantitative comparison with recent MPPT studies

Ref.	Year	Algorithm	Validation	PV power	Tracking time	Efficiency	PSC handling	Platform
[35]	2021	Standard GWO	Simulation + limited HW	200 W	0.8 - 1.2 s	~98%	Moderate	DSP
[32]	2022	Modified GWO	Simulation	1 kW	3.4 s – 5.8 s	~99%	Good	—
[36]	2026	Improved GWO	Simulation	1 kW	0.1 s – 0.4	~99%	Good	—
[37]	2023	Hybrid PSO-GWO	Simulation	320 W	0.1 s – 0.5 s	97.7–98.6%	Good	—
[38]	2025	Improved PSO	Hardware	50 W	4 – 7 s	83–94%	Moderate	dSPACE
[39]	2021	Modified INC	Hardware	80 W	< 0.3 s	PSC case not treated	Poor	MCU
[30]	2023	Enhanced GWO	Simulation	1 kW	0.20 s	~99%	Good	—
This work	2025	IGWO (Sobol + exp. decay + re-init + early stop)	Full real-time hardware	36 W	0.35 - 0.50 s	99.0–99.5%	Good	Arduino Uno (8-bit)

4. CONCLUSION

An IGWO-based MPPT framework was mathematically formulated, computationally optimized, and experimentally validated to address the multi-modal optimization challenges of PV systems under PSC. The proposed algorithm incorporates four key enhancements containing low-discrepancy Sobol sequence initialization, non-linear exponential coefficient decay ($\beta = 2$), dynamic adaptive partial re-initialization triggered by irradiance variation detection ($\Delta P > \gamma$), and a stagnation-based early stopping mechanism. Rigorous experimental testing under STC, multi-peak partial shading, and rapid dynamic irradiance steps yielded. Firstly, the IGWO achieved an average tracking efficiency of 99.0 ± 0.5% under extreme three-peak PSC. Secondly, convergence speed and robustness, corresponding to the tracking convergence time, were limited to 0.35 ± 0.08 s across all shading patterns, representing a 40% to 58% reduction in convergence latency compared to standard GWO (0.8 s) and PSO (0.65 s). Thirdly, local trapping mitigation identified by ten independent experimental trials under multi-peak PSC, the IGWO achieved a global peak identification success rate of 100% (10/10 runs), compared to 80.0% (8/10) for PSO and 60.0% (6/10) for P&O. Finally, steady-state operation without oscillation corresponding the early-stopping criterion effectively limited duty-cycle oscillations upon convergence, restricting steady-state power ripple to less than 0.25% and minimizing thermal stress on the switching MOSFET. The experiment was also limited by the small scale of the low-power prototype (36 W), the accuracy limits of the INA219 sensor (±0.5%), and the fact that performance was validated using controlled step-shading profiles rather than long-term, stochastic natural weather patterns. To offer an economical MPPT solution for resource-constrained solar systems, future work will

migrate the controller to 32-bit ARM architectures to reduce loop execution overhead by over 80% and expand deployment to multi-string arrays and hybrid microgrids.

FUNDING INFORMATION

Authors state no funding involved.

AUTHOR CONTRIBUTIONS STATEMENT

This journal uses the Contributor Roles Taxonomy (CRediT) to recognize individual author contributions, reduce authorship disputes, and facilitate collaboration.

Name of Author	C	M	So	Va	Fo	I	R	D	O	E	Vi	Su	P	Fu
Ilyass Belaalia	✓	✓	✓	✓	✓	✓	✓	✓	✓	✓			✓	
Naima Taifi		✓			✓	✓	✓	✓	✓	✓	✓	✓	✓	
Abdessamad Malaoui		✓			✓	✓	✓	✓		✓	✓	✓	✓	
El Hadi Chahid		✓			✓	✓	✓	✓		✓	✓	✓	✓	

C : **C**onceptualization
M : **M**ethodology
So : **So**ftware
Va : **Va**lidation
Fo : **Fo**rmal analysis
I : **I**nvestigation
R : **R**esources
D : **D**ata Curation
O : Writing - **O**riginal Draft
E : Writing - Review & **E**diting
Vi : **Vi**sualization
Su : **Su**pervision
P : **P**roject administration
Fu : **Fu**nding acquisition

CONFLICT OF INTEREST STATEMENT

Authors state no conflict of interest.

DATA AVAILABILITY

The data that support the findings of this study are available on request from the corresponding author. The data, which contain information that could compromise the privacy of research participants, are not publicly available due to certain restrictions.

REFERENCES

[1] A. Jäger-Waldau, "Snapshot of photovoltaics—February 2020," *Energies*, vol. 13, no. 4, Feb. 2020, doi: 10.3390/en13040930.
[2] A. Jäger-Waldau, "Snapshot of photovoltaics − March 2025," *EPJ Photovoltaics*, vol. 16, 2025, doi: 10.1051/epjpv/2025012.
[3] A. Aslam, N. Ahmed, S. A. Qureshi, M. Assadi, and N. Ahmed, "Advances in solar PV systems: A comprehensive review of PV performance, influencing factors, and mitigation techniques," *Energies*, vol. 15, no. 20, Oct. 2022, doi: 10.3390/en15207595.
[4] T. Imane, C. Mohammed, B. Driss, and Z. Youssef, "Detection and Self-correction of Partial Shading Deficiency on Photovoltaic Installation," 2022, pp. 638–648, doi: 10.1007/978-3-031-02447-4_66.
[5] A. Chellakhi, S. El Beid, M. El Marghichi, and E. M. Bouabdalli, "An amended low-cost indirect MPPT strategy with a PID controller for boosting PV system efficiency," *Results in Engineering*, vol. 24, Dec. 2024, doi: 10.1016/j.rineng.2024.103526.
[6] M. Kermadi *et al.*, "Recent developments of MPPT techniques for PV systems under partial shading conditions: a critical review and performance evaluation," *IET Renewable Power Generation*, vol. 14, no. 17, pp. 3401–3417, Dec. 2020, doi: 10.1049/iet-rpg.2020.0454.
[7] L. Zhao, J. Li, K. Feng, X. Wei, J. Song, and Y. Jiao, "A hybrid optimization algorithm for GWO Fine-tuning GRU-Aided AKF during GPS outage," *Measurement*, vol. 206, p. 112302, Jan. 2023, doi: 10.1016/j.measurement.2022.112302.
[8] A. Ghilani, A. Terki, Z. Alili, A. M. Ghodbane, and O. Belaroussi, "Experimental validation of PSO and GWO-based MPPT for a single-stage three-phase grid-connected PV system under partial shading," *Journal Européen des Systèmes Automatisés*, vol. 57, no. 5, Oct. 2024, doi: 10.18280/jesa.570514.
[9] I. Ait Ayad, E. Elwarraki, and M. Baghdadi, "Intelligent Perturb and Observe Based MPPT Approach Using Multilevel DC-DC Converter to Improve PV Production System," *Journal of Electrical and Computer Engineering*, vol. 2021, pp. 1–13, Feb. 2021, doi: 10.1155/2021/6673022.
[10] S. K. Maitra *et al.*, "Impact of urban density on PV efficiency and battery degradation: a comparative assessment," *International Journal of Advanced Technology and Engineering Exploration*, vol. 12, no. 132, pp. 1686–1699, Nov. 2025, doi: 10.19101/IJATEE.2025.121220264.
[11] N. Qachchachi, H. Mahmoudi, and A. El Hassnaoui, "Control strategy of hybrid AC/DC microgrid in standalone mode," *International Journal of Renewable Energy Development*, vol. 9, no. 2, pp. 295–301, Jul. 2020, doi: 10.14710/ijred.9.2.295-301.
[12] S. Motahhir, A. El Hammoumi, and A. El Ghzizal, "The most used MPPT algorithms: Review and the suitable low-cost embedded board for each algorithm," *Journal of Cleaner Production*, vol. 246, Feb. 2020, doi: 10.1016/j.jclepro.2019.118983.

[13] S. Chtita, S. Motahhir, and A. El Ghzizal, "A new design and embedded implementation of a low-cost maximum power point tracking charge controller for stand-alone photovoltaic systems," *Energy Technology*, vol. 12, no. 4, Apr. 2024, doi: 10.1002/ente.202301324.
[14] S. Chtita *et al.*, "A novel hybrid GWO–PSO-based maximum power point tracking for photovoltaic systems operating under partial shading conditions," *Scientific Reports*, vol. 12, no. 1, Jun. 2022, doi: 10.1038/s41598-022-14733-6.
[15] S. Motahhir, A. El Hammoumi, and A. El Ghzizal, "The most used MPPT algorithms: Review and the suitable low-cost embedded board for each algorithm," *Journal of Cleaner Production*, vol. 246, Feb. 2020, doi: 10.1016/j.jclepro.2019.118983.
[16] D. Shetty and J. N. Sabhahit, "Grey wolf optimization and incremental conductance based hybrid MPPT technique for solar powered induction motor driven water pump," *International Journal of Renewable Energy Development*, vol. 13, no. 1, pp. 52–61, Jan. 2024, doi: 10.14710/ijred.2024.57096.
[17] M. Y. Worku *et al.*, "A comprehensive review of recent maximum power point tracking techniques for photovoltaic systems under partial shading," *Sustainability*, vol. 15, no. 14, Jul. 2023, doi: 10.3390/su151411132.
[18] R. Rajesh and M. Carolin Mabel, "A comprehensive review of photovoltaic systems," *Renewable and Sustainable Energy Reviews*, vol. 51, pp. 231–248, Nov. 2015, doi: 10.1016/j.rser.2015.06.006.
[19] N. A. Kamarzaman and C. W. Tan, "A comprehensive review of maximum power point tracking algorithms for photovoltaic systems," *Renewable and Sustainable Energy Reviews*, vol. 37, pp. 585–598, Sep. 2014, doi: 10.1016/j.rser.2014.05.045.
[20] M. Ilyas, H. Khalifa, and E. Ghazal, "Design of a MPPT system based on modified grey wolf optimization algorithm in photovoltaic system under partially shaded condition," *International Journal of Computer (IJC) International Journal of Computer (IJC*, vol. 40, no. 1, pp. 36–49, 2021.
[21] A. Moulaye Rchid, M. Attia, M. E. MOHAMED MAHMOUD, V. Elvally, Z. Aoulmi, and A. Ould Mahmoud, "Comparative analysis of AI-driven machine learning models for fault detection and maintenance optimization in photovoltaic systems," *Solar Energy and Sustainable Development Journal*, vol. 14, no. 1, pp. 361–378, Apr. 2025, doi: 10.51646/jsesd.v14i1.419.
[22] M. Atillah, H. Stitou, A. Boudaoud, and M. Aqil, "Comparative study of two ANFIS-based MPPT controls under uniform and partial shading conditions," *Solar Energy and Sustainable Development Journal*, pp. 89–103, Dec. 2024, doi: 10.51646/jsesd.v14iSI_MSMS2E.400.
[23] M. Almihat and J. Munda, "Comprehensive review on challenges of integration of renewable energy systems into microgrid," *Solar Energy and Sustainable Development Journal*, vol. 14, no. 1, pp. 199–236, Mar. 2025, doi: 10.51646/jsesd.v14i1.382.
[24] D. Haji and N. Genc, "Dynamic behaviour analysis of ANFIS based MPPT controller for standalone photovoltaic systems," *International Journal of Renewable Energy Research*, vol. 10, no. 1, pp. 101–108, 2020, doi: 10.20508/ijrer.v10i1.10244.g7897.
[25] C. Ben Salah and M. Ouali, "Comparison of fuzzy logic and neural network in maximum power point tracker for PV systems," *Electric Power Systems Research*, vol. 81, no. 1, pp. 43–50, Jan. 2011, doi: 10.1016/j.epsr.2010.07.005.
[26] R. Sangrody, S. Taheri, A.-M. Cretu, and E. Pouresmaeil, "An Improved PSO-Based MPPT Technique Using Stability and Steady State Analyses Under Partial Shading Conditions," *IEEE Transactions on Sustainable Energy*, vol. 15, no. 1, pp. 136–145, Jan. 2024, doi: 10.1109/TSTE.2023.3274939.
[27] M. V. da Rocha, L. P. Sampaio, and S. A. Oliveira da Silva, "Comparative analysis of ABC, Bat, GWO and PSO algorithms for MPPT in PV systems," in *2019 8th International Conference on Renewable Energy Research and Applications (ICRERA)*, IEEE, Nov. 2019, pp. 347–352, doi: 10.1109/ICRERA47325.2019.8996520.
[28] A. Nouh, A. Almalih, M. Faraj, A. Almalih, and F. Mohamed, "Hybrid of meta-heuristic techniques based on cuckoo search and particle swarm optimizations for solar PV systems subjected to partially shaded conditions," *Solar Energy and Sustainable Development Journal*, vol. 13, no. 1, pp. 114–132, Mar. 2024, doi: 10.51646/jsesd.v13i1.178.
[29] C. S. Kumar and R. S. Rao, "A novel global MPP tracking of photovoltaic system based on whale optimization algorithm," *International Journal of Renewable Energy Development*, vol. 5, no. 3, pp. 225–232, Nov. 2016, doi: 10.14710/ijred.5.3.225-232.
[30] I. Belaalia, N. Taifi, A. Malaoui, and K. Taifi, "MPPT command enhancement based on an ameliorated grey wolf optimization algorithm for a standalone PV system," *International Journal of Advanced Technology and Engineering Exploration*, vol. 10, no. 109, pp. 1696–1712, Dec. 2023, doi: 10.19101/IJATEE.2023.10102040.
[31] S. Mirjalili, S. M. Mirjalili, and A. Lewis, "Grey wolf optimizer," *Advances in Engineering Software*, vol. 69, pp. 46–61, Mar. 2014, doi: 10.1016/j.advengsoft.2013.12.007.
[32] D. J. K. Kishore, M. R. Mohamed, K. Sudhakar, and K. Peddakapu, "An improved grey wolf optimization based MPPT algorithm for photovoltaic systems under diverse partial shading conditions," *Journal of Physics: Conference Series*, vol. 2312, no. 1, p. 012063, Aug. 2022, doi: 10.1088/1742-6596/2312/1/012063.
[33] S. Motahhir, S. Chtita, A. Chouder, and A. El Hammoumi, "Enhanced energy output from a PV system under partial shaded conditions through grey wolf optimizer," *Cleaner Engineering and Technology*, vol. 9, Aug. 2022, doi: 10.1016/j.clet.2022.100533.
[34] D. Shetty and J. N. Sabhahit, "Grey wolf optimization and incremental conductance based hybrid MPPT technique for solar powered induction motor driven water pump," *International Journal of Renewable Energy Development*, vol. 13, no. 1, pp. 52–61, Jan. 2024, doi: 10.14710/ijred.2024.57096.
[35] A. F. Mirza, Q. Ling, M. Y. Javed, and M. Mansoor, "Novel MPPT techniques for photovoltaic systems under uniform irradiance and Partial shading," *Solar Energy*, vol. 184, pp. 628–648, May 2019, doi: 10.1016/j.solener.2019.04.034.
[36] R. Celikel, O. Aydogmus, and M. Yilmaz, "An improved grey wolf optimization-based MPPT algorithm for photovoltaic systems under partial shading conditions," *Scientific Reports*, vol. 16, no. 1, p. 16671, Apr. 2026, doi: 10.1038/s41598-026-45860-z.
[37] Hassan S. Ahmed, Ahmed J. Abid, Adel A. Obed, Ameer L. Saleh, and Reheel J. Hassoon, "Maximizing Energy Output of Photovoltaic Systems: Hybrid PSO-GWO-CS Optimization Approach," *Journal of Techniques*, vol. 5, no. 3, pp. 174–184, Sep. 2023, doi: 10.51173/jt.v5i3.1312.
[38] M. K. A. Mohd Jamhari, N. Hashim, R. Baharom, and M. M. Othman, "Simulation and verification of improved particle swarm optimization for maximum power point tracking in photovoltaic systems under dynamic environmental conditions," *International Journal of Power Electronics and Drive Systems (IJPEDS)*, vol. 16, no. 1, Mar. 2025, doi: 10.11591/ijpeds.v16.i1.pp608-621.
[39] D. Ounnas, D. Guiza, Y. Soufi, and M. Maamri, "Design and Hardware Implementation of Modified Incremental Conductance Algorithm for Photovoltaic System," *Advances in Electrical and Electronic Engineering*, vol. 19, no. 2, Jul. 2021, doi: 10.15598/aeee.v19i2.3881.

BIOGRAPHIES OF AUTHORS



Ilyass Belaalia is a researcher working at the intersection of clean energy and smart technologies. He received his bachelor's degree in electrical engineering in 2014 and his master's degree in renewable energy engineering in 2019, both from Sultan Moulay Slimane University, Morocco. He is currently pursuing a Ph.D. degree at the same university in Beni Mellal, Morocco. His research interests include artificial intelligence and computer science, particularly their applications in developing sustainable energy solutions. He can be contacted at email: ilyass.belaaliafpb@usms.ac.ma.



Naïma Taifi is a professor specializing in measurement, control, and electronic instrumentation in electrical engineering. She received her bachelor's degree from Sultan Moulay Slimane University, Morocco, in 1998; her master's degree from Chouaib Doukkali University, Morocco, in 2001; and her Ph.D. degree from Ibn Zohr University, Morocco, in 2006. Her doctoral research focused on the application of ultrasonic techniques to the control of agri-food processes, particularly milk coagulation and fish freezing and thawing. She has authored more than 10 scientific publications and delivered 20 conference presentations, making contributions to the fields of instrumentation and control engineering. She can be contacted at email: taifinaima@yahoo.fr.



Abdessamad Malaoui has been a senior lecturer at Sultan Moulay Slimane University, Beni Mellal, Morocco, since 2006. He received his Ph.D. degree in electrical and power engineering from Aix-Marseille University, France, in 2006. His areas of expertise include electronics, signal processing, thin films, and renewable energy. He has authored more than 130 scientific publications. He is a member of the International Federation of Global and Green Information and Communication Technology (IFGICT), USA. He also serves as the president of the university's Commission on Renewable Energy, Energy Efficiency, and Digital Transformation, and as the vice-president of the Sahara Forum for Dialogue and Cultures. In addition, he coordinates the Master's programme in Renewable Energy Engineering and Energy Efficiency and the Professional Bachelor's programme in Irrigation Techniques and Renewable Energies. He can be contacted at email: a.malaoui@usms.ma.



El Hadi Chahid is currently a university professor at the Regional Center for Education and Training Professions (CRMEF) of Marrakech-Safi, Morocco. He obtained his Habilitation à Diriger des Recherches (HDR) from the National School of Applied Sciences, Ibn Zohr University, Agadir, Morocco, in 2018. His research interests include materials science for solar cells, renewable energy, and electronic engineering. He can be contacted at email: chahid2016@yahoo.com.